Science of the Total Environment 887 (2023) 164000

Contents lists available at ScienceDirect

Science of the Total Environment

journal homepage: www.elsevier.com/locate/scitotenv

PPCPs abatement using TiO_2-based catalysts by photocatalytic oxidation and ozonation: The effect of nitrogen and cerium loads on the degradation performance and toxicity impact

Eva Domingues [a], Fátima Jesus [b], Mariana Alvim [a], Carla Cotas [a], Pawel Mazierski [c], Joana L. Pereira [b], João Gomes [a,*]

[a] University of Coimbra, CIEPQPF – Chemical Engineering Processes and Forest Products Research Center, Department of Chemical Engineering, Faculty of Sciences and Technology, Rua Sílvio Lima, 3030-790 Coimbra, Portugal

[b] CESAM - Centre for Environmental and Marine Studies, Department of Biology, University of Aveiro, Campus de Santiago, 3810-193 Aveiro, Portugal

[c] Faculty of Chemistry, Department of Environmental Technology, University of Gdańsk, 80-308 Gdańsk, Poland

HIGHLIGHTS

- Doped TiO_2 catalyst revealed low efficiency for PPCPs removal through photocatalysis.
- Precursors load can promote the ecotoxicity of treated solutions from leaching.
- Photocatalytic ozonation removed the PPCPs but in some cases increase the ecotoxicity.
- Photocatalytic ozonation showed better ecotoxicological results than photocatalysis.

GRAPHICAL ABSTRACT

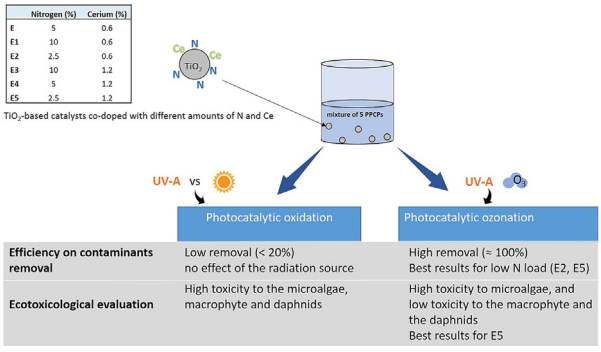

ARTICLE INFO

Editor: Damià Barceló

Keywords:
Contaminants of emerging concern
Photocatalytic oxidation
Photocatalytic ozonation
Doping TiO_2
Ecotoxicity

ABSTRACT

Pharmaceutical and personal care products (PPCPs) have been consumed in great extension and most of these are found in water bodies, owing to the inefficiency of conventional wastewater treatments. To face against these recalcitrant contaminants, advanced oxidation processes such as photocatalysis and ozonation have been studied. Moreover, the combination of these technologies can improve the degradation of PPCPs, reducing the ozone consumption and the effluent toxicity with the presence of photocatalysts. In particular, this study aimed to evaluate the effects of different N and Ce loads in co-doping TiO_2 catalysts on the efficiency of photocatalytic oxidation and photocatalytic ozonation for PPCPs abatement, as well as on the resultant toxicity to aquatic species. Different radiation sources (UVA and solar radiation) were considered for the photocatalytic oxidation. A mixture of 5 PPCPs: paracetamol, sulfamethoxazole, carbamazepine, methylparaben and propylparaben was used as a model synthetic effluent. Photocatalysis showed a low efficiency on the PPCPs removal (<20 %), which was not affected by the radiation source. In general, the tested catalysts showed no or low added-value for reducing the toxicity of the synthetic effluent. Concerning photocatalytic ozonation, the lowest N amount (2.5 % w/w) promoted the best results for PPCPs removal, achieving values up to 100 % with significant reduction of ozone dose compared to photolytic ozonation. In general, photocatalytic ozonation showed better ecotoxicological performance than single photocatalysis. Compared to single photolytic ozonation, a benefitial effect was observed for two aquatic species, using a specific catalyst. This catalyst, prepared by doping TiO_2 with 2.5 % w/w N and 1.2 % w/w Ce, showed to be the most promisong one, with potential to be used in

* Corresponding author.
E-mail address: jgomes@eq.uc.pt (J. Gomes).

http://dx.doi.org/10.1016/j.scitotenv.2023.164000
Received 21 January 2023; Received in revised form 28 April 2023; Accepted 4 May 2023
Available online 9 May 2023

photocatalytic ozonation. Hence, this work highlights the potential role of N and Ce co-doped TiO_2-based catalysts in photocatalytic ozonation for wastewater treatment.

1. Introduction

Contaminants of emerging concern (CECs) are a wide range of compounds that are starting to be monitored, and which may cause adverse effects to the environment and human health (Eggen et al., 2014; Taheran et al., 2018). Many CECs present high persistency and recalcitrant character, and have proven to be mutagenic, carcinogenic or have reproductive toxicity (Walker, 2014; Cvetnic et al., 2019). Among other CECs, pharmaceutical and personal care products (PPCPs) are described as micropollutants due to their presence in the environment at very low concentrations (ng/L to μg/L) (Ahmed et al., 2017; Lincho et al., 2021). Owing to the limitations of the conventional wastewater treatment technologies, these compounds have been detected worldwide, with increased concentrations along the years (Ahmed et al., 2017; Salimi et al., 2017). The exponential growth of population and water scarcity are the major causes of this augmentation. In fact, the growth of population contributes to the increase in the PPCPs consumption which will be released mainly as domestic effluents, ended up reaching the aquatic systems. Moreover, the water scarcity will promote the reduction of water quality due to the presence of such contaminants. The traditional wastewater treatment plants cannot remove such recalcitrant compounds due to the biorefractory character (Rizzo et al., 2019). Hence, it is relevant to improve the wastewater treatments efficiency envisaging the complete removal of PPCPs and the toxicity reduction.

As an alternative, advanced oxidation processes (AOPs), namely photocatalytic processes and ozonation, appear to be a promising technology to eliminate these PPCPs (Rodriguez-Narvaez et al., 2017; Rizzo et al., 2019). These processes involve the production of different radicals (e.g. $OH^{\bullet}$, $HOO^{\bullet}$, $O_3^{\bullet-}$) capable to degrade a large variety of organic molecules. AOPs have proven to be highly effective and to have low detrimental impact on the environment, but the operational conditions need to be optimized. Besides the usage of these single methods, such as ozonation and photocatalysis, combinations among them can present higher degradation rates of a broader range of PPCPs. In particular, the combination of ozonation and photocatalysis can be a promising method to improve the PPCPs abatement by mineralization (Mehrjouei et al., 2015).

Ozone is a powerful oxidant that can be used for the abatement of PPCPs (Gomes et al., 2017). However, due to its selective character, it can produce refractory compounds which can be more problematic than the initial PPCPs (Gomes et al., 2019b). Ozone, being an electrophilic species, acts as an electron acceptor, which can reduce the electron-hole recombination of the photocatalysts and adsorb on its surface, producing more radicals (Xiao et al., 2015).

Photocatalysis requires the use of a semiconductor, and the most common is titanium dioxide (TiO_2) due to its low cost, high stability properties and photoactivity (Pelaez et al., 2012; Velegraki et al., 2015). However, one of the major drawbacks of TiO_2 is that, with a bandgap energy of 3.2 eV, only ultraviolet (UV) radiation is capable to activate it under the 300–390 nm wavelength (Pelaez et al., 2012; Centi and Perathoner, 2014; Gomes et al., 2019a). Thus, mechanisms to decrease the bandgap energy of TiO_2 and shift its activity into the visible radiation spectrum (>400 nm) are important to make photocatalytic-based processes more efficient and cheaper, allowing their use with the solar radiation. In this sense, doping and co-doping have become techniques of high interest. These techniques comprise the incorporation of different elements, such as metal (e.g. Cu, Fe, Mn, Ce) and non-metal (e.g. N, B, C, S) elements, capable to interact with the conduction and valence band of the semiconductor reducing its bandgap energy (Pham and Lee, 2017; Rimoldi et al., 2018). The application of nitrogen for the doping of TiO_2 proved to increase the photoactivity for the visible or solar radiation (Petala et al., 2015; Rimoldi et al., 2018). For instance, Solís et al. (2015) used the N-TiO_2 in the photocatalytic ozonation process for the abatement of an herbicide, with suitable improvement in the ozone activity. In addition, in a previous work of our group (Fernandes et al., 2020a), N-TiO_2 catalysts showed better performance on the degradation of a parabens mixture than the pristine TiO_2 catalyst. The co-doping with Ce can also improve ozonation since Ce oxides have high catalytic activity towards ozone, enhancing the ozone decomposition (Nawrocki, 2013; Qi et al., 2020). However, the combination of both N and Ce onto TiO_2-catalysts has not been thoroughly explored, despite the individual results pointing it as a promising combination to apply on the photocatalysis and photocatalytic ozonation of several PPCPs (Fernandes et al., 2020a). For instance, it is not known what is the best load of each element towards a better degradation performance and a lower environmental impact. Shen et al. (2009) reported that co-doping a TiO_2 catalyst with N and Ce (at 0.02 and 0.01 M ratio, respectively) improved nitrobenzene removal by photocatalysis under visible light. Moreover, Charanpahari et al. (2013) analyzed the photocatalytic degradation of methyl orange, and reported a beneficial effect of doping TiO_2 catalysts with Ce, N and S, due to synergistic effects among the multiple dopants. Compared to the previously mentioned studies, the present study shows an integrative approach by considering not only the effects on the PPCPs removal (both upon photocatalysis and photocatalytic ozonation) but also the ecotoxicological consequences.

Hence, this work aims to evaluate the effects of different N and Ce loads in the co-doping of TiO_2 catalysts on the efficiency of photocatalytic oxidation and photocatalytic ozonation for PPCPs abatement, as well as on the resulting toxicity to aquatic species. A synthetic effluent was used, consisting on a mixture of diverse PPCPs namely paracetamol (PCT, analgesic), sulfamethoxazole (SMX, antibiotic), carbamazepine (CBZ, anticonvulsant), methylparaben and propylparaben (MP and PP, respectively, two common parabens). A two-step procedure was used. First, the efficiency of TiO_2 catalysts doped with different N loads (2.5, 5 and 10 % w/w) and co-doped with Ce (0.6 and 1.2 % w/w) was assessed on the removal of the PPCPs, considering both photocatalysis and photocatalytic ozonation. Moreover, two different radiation sources were considered in the photocatalysis - UVA and solar radiation. Second, the ecotoxicological effects of those catalysts, used in photocatalysis (solar radiation) and photocatalytic ozonation (UVA radiation) were assessed to aquatic species. The selected model species were the microalga *Raphidocelis subcapitata*, the macrophyte *Lemna minor*, and the crustacean *Daphnia magna*. As far as the authors know, this work is the first to address the effects of N and Ce loads in co-doping of TiO_2 catalysts for abatement of PPCPs, and also the first to consider the degradation effects both in photocatalysis and photocatalytic ozonation. Moreover, this work presents an integrated assessment of such effects by addressing the ecotoxicological impact of the different loads of N and Ce.

2. Materials and methods

2.1. Synthetic effluent preparation

The synthetic effluent was prepared by dissolving methylparaben (MP), propylparaben (PP), paracetamol (PCT), sulfamethoxazole (SMX) and carbamazepine (CBZ) in ultrapure water, at 1 mg/L each. These PPCPs were acquired to Sigma-Aldrich (≥ 99 % purity).

2.2. Preparation of catalysts

The catalysts were prepared by the sol-gel method, following Fernandes et al. (2020a). Titanium (IV) butoxide (97 % purity), used as titanium

dioxide precursor, was obtained from Aldrich Chemical. Urea and cerium (III) nitrate hexahydrate, used as nitrogen and cerium precursors respectively, were acquired to Sigma-Aldrich.

The preparation involved two different solutions. The first solution consisted on diluting titanium butoxide in absolute ethanol (1:5 v/v, respectively), stirring during 30 min. The second solution was composed by distilled water, absolute ethanol, acid acetic glacial, urea and cerium nitrate hexahydrate according to its respective ratio 2.5 % w/w, 5 % w/w, 10 % w/w for nitrogen and 0.6 % w/w and 1.2 % w/w for cerium. After homogenization of the second solution, it was added dropwise to the first solution. The resulting solution was kept under aging during 2 h at room temperature. Then the solution was placed at 70 °C during about 12 h to evaporate the solvent. The final step was the calcination stage, which was performed during 3 h at 450 °C, followed by cooling and manual milling. Six different catalysts were produced, and their composition in terms of nitrogen and cerium is presented in Table 1.

2.3. Advanced oxidation processes

The test solutions that were submitted to the advanced oxidation processes were obtained by adding the prepared catalyst to the mixture of 5 PPCPs, at a concentration of 100 mg/L.

The experimental procedure involved two different technologies: photocatalytic oxidation and photocatalytic ozonation. The photocatalytic oxidation was performed with two different radiations sources: UVA and sunlight radiation, during 120 min. The experiments under UVA radiation were carried out in a 2 L glass reactor under constant stirring at 700 rpm equipped with 3 UVA lamps (Philips TL 6 W BLB, the peak emission at 365 nm) and with a thermostatic bath at 25 °C. The solar experiments were performed at the Department of Chemical Engineering of the University of Coimbra (40.186622°, −8.4182372°) in a beaker of 200 mL with magnetic stirring at 300 rpm. These experiments were made in July 2022 and the average solar radiation power was around 700 ± 150 W/m^2 during the experiments. All the experiments were performed in duplicate.

The photocatalytic ozonation experiments of each catalyst were carried out in the same reactor previously described for the photocatalytic oxidation under UVA radiation described above. Ozone was produced from pure oxygen (99.9 %) using an ozone generator (802 N, BMT). The inlet gas flowrate (Q_{gas}) was 0.2 L/min over the volume solution (V_{liq}), and the inlet ($[O_3]_i$) and outlet ($[O_3]_o$) ozone concentrations were followed by gas analyzers (BMT 963 and 964, respectively). The transferred ozone dose (TOD), in mg O_3/L, was estimated through the Eq. (1).

$$TOD = \int_0^t \frac{Q_{gas}}{V_{liq}} \times \left([O_3]_i - [O_3]_o\right) \times dt \quad (1)$$

2.4. Ecotoxicity evaluation

The ecotoxicity of the synthetic effluent after treatment by photocatalysis oxidation using solar radiation and by photocatalytic ozonation (UVA radiation) using the co-doped titanium dioxide (nitrogen and cerium) catalysts was determined for *R. subcapitata*, *L. minor* and *D. magna*.

Since the synthetic effluent does not fulfill the species requirements for survival and growth, namely macro and micronutrients, the samples were spiked with nutrients previously to the experiments to attain the same nutrient levels as in their standard medium. Nutrient spiking caused a slight dilution of the sample, as mentioned below. This procedure was required to ensure that the observed ecotoxicological effects were not due to nutrient scarcity.

The ecotoxicity of the untreated synthetic effluent was also evaluated, as well as that of the photolytic ozonation treatment per se (no catalysts). This aimed to allow further comparisons among treatments and support illations.

Table 1
Composition and designation of the prepared catalysts.

Name	Nitrogen (% w/w)	Cerium (% w/w)
E	5	0.6
E1	10	0.6
E2	2.5	0.6
E3	10	1.2
E4	5	1.2
E5	2.5	1.2

2.4.1. Raphidocelis subcapitata

Growth inhibition tests with *R. subcapitata* were performed according to the OECD guideline 201 (OECD, 2011), with the modifications described by Gomes et al. (2019b). Experiments were carried out in 24-well microplates. Each sample was tested in triplicate and initiated with 1 × 10^4 cells/mL. The microalgae originated from a laboratory culture maintained in Woods Hole MBL medium (Stein, 1979), at 20 °C ± 1 °C under a 16 h light:8 h dark photoperiod. Nutrient spiking of the samples was performed to comply with the MBL medium recipe, resulting in each sample being tested at 98.2 % strength. A control treatment was also carried out consisting of ultrapure water, nutrient spiking and microalgae. A 96 h exposure period was allowed, at 23 °C ± 1 °C and continuous light supply. After this period, algal density was determined by measuring the absorbance of each sample at 440 nm. The absorbance values were converted to cell density values using a previously defined curve, and the latter were then used to determine the biomass yield following the OECD guideline 201 (OECD, 2011).

2.4.2. Lemna minor

Growth inhibition tests with L. *minor* were performed according to the OECD guideline 221 (OECD, 2006), with the modifications described by Gomes et al. (2019b). Each sample was tested in triplicate. Tests were carried out in 6-well microplates and initiated with 3 colonies with a total of 10 fronds per replicate. Colonies were obtained from laboratory cultures maintained in Steinberg medium at 20 °C ± 1 °C under a 16 h light:8 h dark photoperiod. Nutrient spiking was performed to comply with the Steinberg medium recipe, resulting in each sample being tested at 93.5 % strength. A control treatment was also carried out consisting of ultrapure water, nutrient spiking and the colonies. A 7 d exposure period was allowed, at 23 °C ± 1 °C and continuous light supply. After this period, the number of fronds per well was counted and the macrophytes were dried at 60 °C for quantification of their dry weight. The number of fronds and the dry weight were used to determine the yield inhibition, according to the OECD guideline 221 (OECD, 2006).

2.4.3. Daphnia magna

Immobilization tests with *D. magna* were performed according to the OECD guideline 202 (OECD, 2004) with the modifications described by Gomes et al. (2019b). Experiments were carried out in glass test tubes. Each sample was tested in quadruplicate, using 5 neonate daphnids (<24 h old) per replicate. Neonates were obtained from laboratory cultures, which were maintained in ASTM hard water (ASTM, 2004) enriched with an organic additive extracted from *Ascophyllum nodosum* and fed every other day with *R. subcapitata* at 3.0 × 10^5 cells/mL. Temperature was kept at 20 °C ± 1 °C and the photoperiod was 16 h light:8 h dark, both for cultures and during the experiments. Nutrient spiking was performed to comply with the ASTM hard water recipe, resulting in each sample being tested at 92.0 % strength. A control treatment was also carried out consisting of ultrapure water, nutrient spiking and the neonate daphnids. No food was supplied. After 48 h of exposure, the immobilized daphnids in each tube were counted, and used to determine the percentage of immobilization.

2.5. Analytical procedures

The UV–Vis Diffuse Reflectance Spectroscopy (DRS) spectra for solid catalysts was performed by a Jasco V-650 spectrophotometer for the wavelength range of 250 to 600 nm. The band gap energy of all catalysts was calculated using Tauc's plot as $(\alpha h\upsilon)^n$ versus $h\upsilon$, based on Tauc's rule:

$$(\alpha h\upsilon)^n = B\left(h\upsilon - E_{bg}\right)^n \quad (2)$$

where α is the absorption coefficient, B is an energy independent constant, h is the Planck's constant, υ is the light frequency and n indicates the type of optical transition, which is n = 1/2 for direct allowed transition (Shkir and Yahia, 2018). The band gap of each catalyst was obtained by the intersection point of the tangent line where $(\alpha h\upsilon)^{1/2}$.

The surface morphology and chemical structure of the prepared catalysts were examined using field-emission scanning electron microscopy (FE-SEM, JEOL JSM-7610 F) and Raman spectroscopy, respectively, at room temperature (Thermo Scientific DXR Smart Raman spectrometer with a 532 nm laser). BET surface area, total pore volume and pore size distribution were estimated from nitrogen adsorption-desorption isotherms conducted on a Micro 200 (3P Instruments) at a temperature of −196.2 °C. *prior* to the measurements, the samples were degassed with nitrogen gas at 200 °C for 5 h. Micropore analysis was done by HK/SF method. Photoluminescence measurements were conducted at room temperature using a LS-50B Luminescence Spectrophotometer, with a Xenon discharge lamp as an excitation source and a R928 photomultiplier as a detector. The samples were excited at 300 nm, and the excitation radiation was directed onto the sample surface at a 90° angle.

The X-ray diffraction (XRD) analysis was made through a diffractometer (Bruker D8 Advance) for the pristine TiO_2 and the E (0.6 % Ce + 5 % N) catalysts for crystalline phases identification. The diffractometer works with Cu Kα radiation (2.2 kW ceramic tube), equipped with a 1D LynxEye detector (Silicon Drift Detector) covering an angle of ~3° and with ~25 % energy resolution.

The contaminants concentration along the oxidation reactions was followed through the high-performance liquid chromatography (HPLC), a Beckman Coulter Gold system. The mobile phase (1 mL/min) consisted of a mixture of 50:50 methanol: acidic water (0.1 % orthophosphoric acid). The injection volume was 100 μL and chromatography column was a C18 (SiliaChrom) at 40 °C. The detection of SMX was performed at λ = 280 nm while for parabens, CBZ, and PCT was made at λ = 255 nm.

2.6. Data analysis

The data analysis was performed using the free software Gretl. A total of 12 experiments for the degradation of PCT by photocatalytic oxidation were analyzed, representing the results obtained for the catalysts presented in Table 1 with two different radiations sources: UVA and solar radiation. PCT was chosen for this analysis as this contaminant, along with CBZ and SMX, showed the highest abatement, whereas the removal of the remaining PPCPs (MP and PP) was lower.

The application of data analysis is very advantageous to optimize the number and costs of experiments. By an exploratory analysis, important knowledge can be obtained to better describe the response of the degradation of PCT with different catalysts and radiation sources. In the present work, data analysis was conducted through a correlation matrix to examine the correlation level between the degradation of PCT, different catalysts and radiation sources. The correlation coefficients were used as indication of the level of dependence between variables. For the model development, linear regression with multiple variables was used to adjust the degradation of PCT. However, for the analysis presented in this work, the build of model for the degradation of PCT has to be carefully analyzed. Moreover, the representation of experimental data and model metrics needs to be used to compare between model adjustments.

The statistical analysis of ecotoxicological data was carried out with a one-way ANOVA. Whenever the data did not verify the ANOVA assumptions (normality assessed through the Shapiro-Wilk test, and homoscedasticity assessed through the Brown-Forsythe test), the Kruskal-Wallis test was used. To compare the differences of catalysts among each other, the pairwise multiple comparison Tukey Test was used. The existence of significant differences between the treatments with the catalysts and the untreated synthetic effluent, as well as between the catalysts and the photolytic ozonation was assessed using the multiple comparisons Dunnett's test. A *p*-value of 0.05 was used for all statistical analyses.

3. Results and discussion

3.1. UV–vis DRS analysis of the catalysts

The co-doping effect using N and Ce over TiO_2 was assessed for all the catalysts through the UV–Vis DRS analysis. This analysis measured the potential of catalysts to absorb the radiation sources used in this work, UVA and solar radiation. Fig. 1 presents the absorption spectrum from UV–Vis DRS and the Tauc's plot analysis for all the prepared catalysts.

The used N and Ce amounts for the doping of TiO_2 did not promote differences on the absorbance spectrum along the wavelength as can be seen in the Tauc's plot (Fig. 1A,B). Considering the absorption spectrum for all

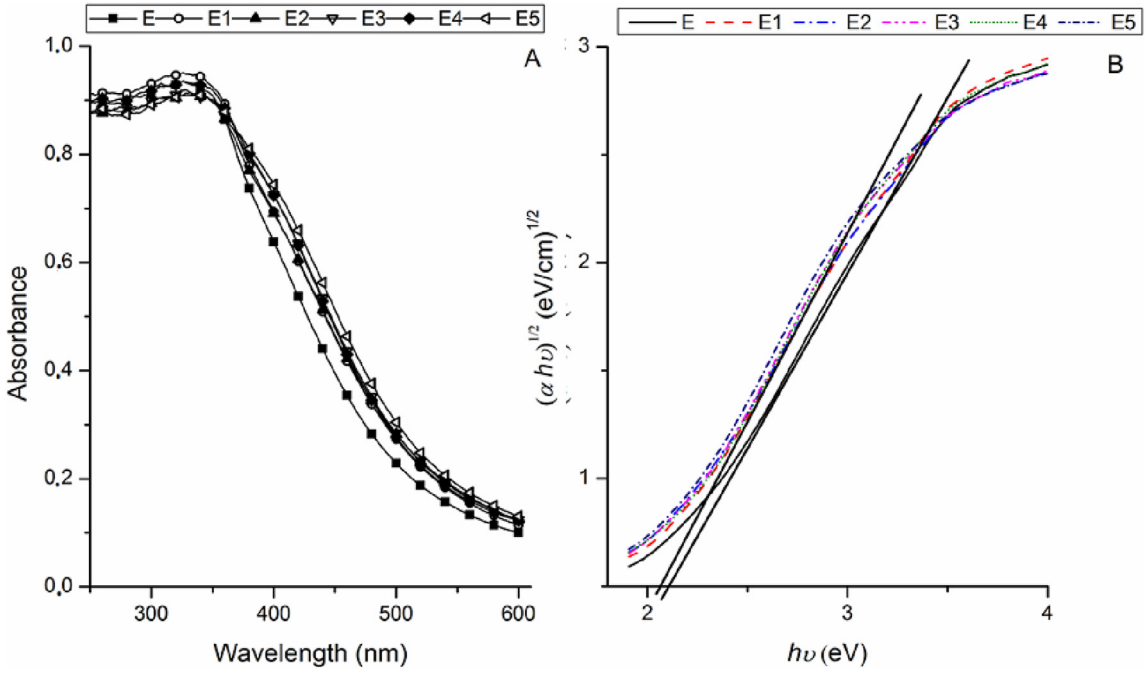

Fig. 1. UV–Vis diffuse reflectance spectroscopy (DRS) spectra (A) and Tauc's plot (B) of the tested catalysts.

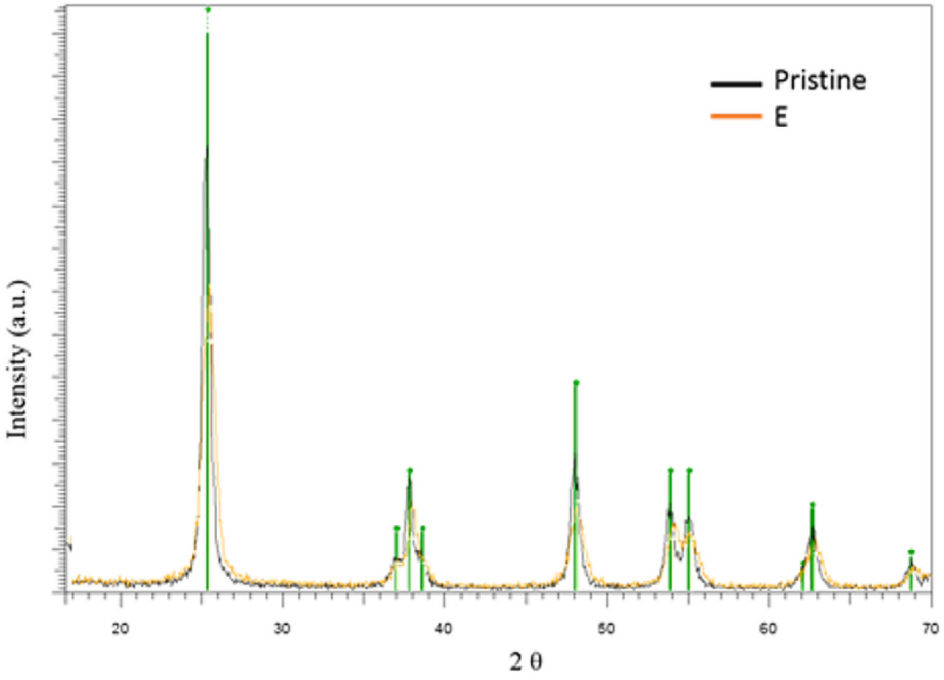

Fig. 2. XRD analysis of the bare TiO_2 (pristine) and the E (0.6 % Ce + 5 % N) catalysts.

the catalysts, it is possible to estimate the energy of the bandgap (Eg) from the following equation (Eq. (3)) (O'Regan and Gratzel, 1991):

$$Eg = \frac{1240}{\lambda} \quad (3)$$

where λ is the absorption edge wavelength. Based on Fig. 1B, the energy bandgap was about 2.1 eV for the E catalyst and there were no relevant differences among the prepared catalysts which present a band gap of 2.08 eV. The main crystalline phases of TiO_2 is the anatase and rutile, for which the energy bandgap is about 3.2 eV and 3.0 eV, respectively (Pelaez et al., 2012; Gomes et al., 2019a). However, the doping with Ce and N can promote a significant decrease of the bandgap energy, as shown in previous works (Shen et al., 2009; Sun et al., 2010).

From the XRD analysis (Fig. 2) it is concluded that anatase is the unique crystalline phase present. Moreover, the calcination temperature (450 °C) used during the production of catalysts points to the same conclusion. Sun et al. (2010) analyzed the effect of the calcination temperature over the TiO_2 phases for the different sol-gel prepared Ce/N-TiO_2 catalysts, concluding that from 370 to 420 °C the amorphous phase of TiO_2 converts to anatase phase and the rutile conversion occurs at the range from 550 to 620 °C (Sun et al., 2010). Hence, considering the calcination temperature used in the production of the tested catalysts, it may be assumed that the anatase was the only phase present in the catalysts.

The XRD analysis revealed that anatase is the TiO_2 crystalline phase, as given by the identified peaks at Fig. 2. However, the intensity of peaks clearly decreased for the doped catalyst compared to the pristine TiO_2 (Fig. 2). In fact, the lower intensity and broader peaks can be related to the presence of the amorphous phase which will likely be responsible for the decrease in the photoactivity (Kalantari et al., 2016; Qiu et al., 2019). Moreover, the broader intensity of the first diffraction peak at the angle 25.3° corresponding to the (101) plane indicates the lower crystallite size for the anatase phase (Qiu et al., 2019). Typically, the N and Ce co-doping of TiO_2 can create a small shift in the (1 0 1) diffraction peak (Sun et al., 2010; Lee et al., 2013) but that was not observed in the present study. Moreover, the increased amount of Ce and N can promote broader and lower intensity peaks (Sun et al., 2010; Lee et al., 2013), which agrees with our results (Fig. 2). In order to confirm these results, the Raman analysis was made for all the prepared catalysts (Fig. 3).

Raman spectra was composed of six Raman active modes A1g + 2B1g + 3Eg located at 144, 194, 397, 513, 517 and 639 cm^{-1}, as shown in Fig. 3 (Fan et al., 2016). Ti—O stretching vibration are typically assigned to bands at 517 and 397 cm^{-1}, while bands at 639 cm^{-1} are associated with the O–Ti–O type vibration (Fan et al., 2016; Touati et al., 2016).

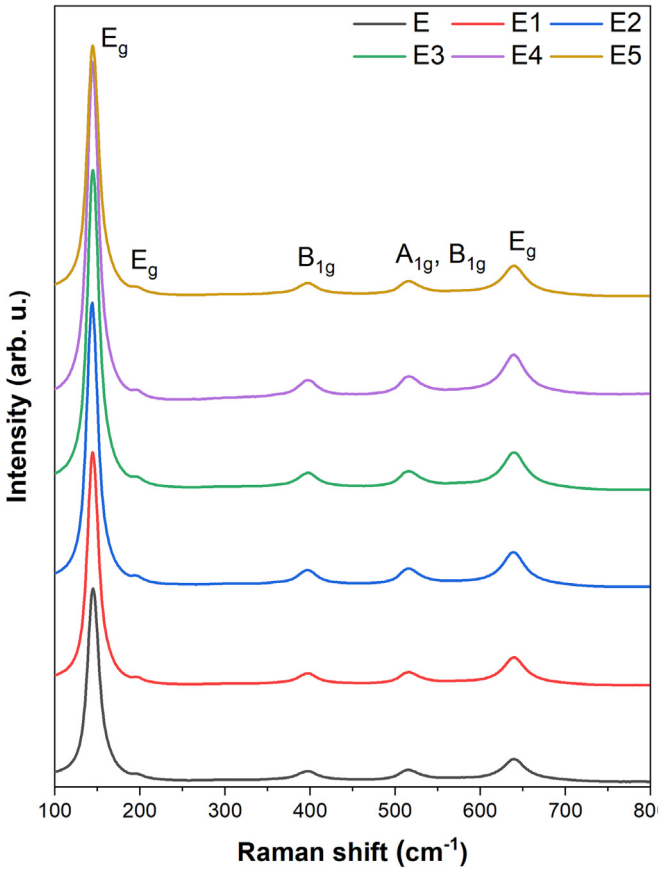

Fig. 3. Raman spectra of the prepared catalysts.

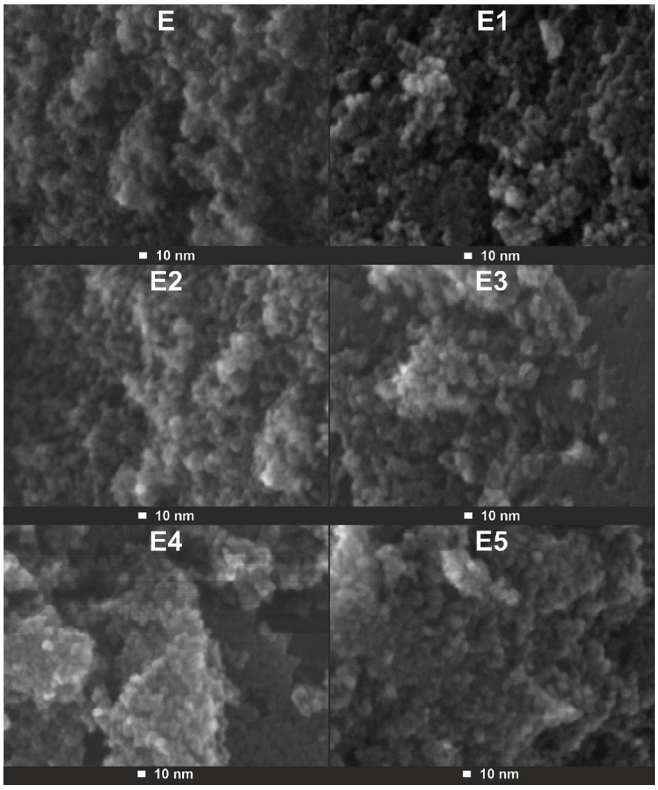

Fig. 4. HR-SEM images of prepared catalysts.

The presence of these Raman modes confirms anatase crystalline form of prepared catalysts (Touati et al., 2016). The results of Raman spectroscopy were in line with the XRD results (Fig. 2).

Surface morphology of the obtained catalysts is shown in Fig. 4. It can be observed that the samples exhibited morphologies of spherical nanoparticles (NPs). The increase in the content of N or Ce did not result in the transformation of NPs into other forms such as nanorods, nanospheres, nanowires. Particle size calculated based on HRSEM images in summarized in Table 2. The use of the sol-gel method to obtain doped TiO_2 made it possible to obtain aggregates of NPs with a size below 10 nm. In both cases (for Ce amount of 0.6 and 1.2 % w/w), an increase in the N content resulted in an increase in the size of the TiO_2 NPs, which is in line with the previous literature (Sun et al., 2010; Lee et al., 2013). It can also be seen that an increase in Ce content from 0.6 to 1.2 % w/w caused formation of bigger NPs.

Table 2 presents the results of the influence of N and Ce doping on the BET surface area, which was determined through liquid nitrogen adsorption-desorption isotherms. The decrease in BET surface area, as observed in Table 2, was found to be caused by an increase in N content leading to an increase in NP size. This increase in size can be attributed to interstitial doping, where N atoms occupy interstitial spaces instead of crystal lattice positions (Ding and Li, 2015). However, it is worth emphasizing that the BET surface area of the modified catalysts is almost twice bigger compared to pristine TiO_2 (66.8 m^2/g, please see the reference (Fernandes et al., 2020a). The increase in N content appears to have a significant impact on total pore volume. The size of the nanoparticles may be responsible for the decrease in total pore volume observed with an increase in N content. It could be also seen that the BET surface area and pore parameters decreased as the Ce content was increased from 0.6 to 1.2%w/w.

Table 2
Particle size, BET surface area and micropore Analysis.

	Average particle size based on SEM images (nm)	BET surface area (m^2/g)	Total pore volume (cm^3/g)	Micropore analysis		
				Micropore volume (cm^3/g)	Most Frequent Pore Diameter (nm)	Median Pore Diameter (nm)
E	7.6 ± 0.5	117.1	0.2211	0.053	0.65	0.75
E1	9.3 ± 0.7	108.8	0.1882	0.053	0.66	0.78
E2	6.3 ± 0.6	136.4	0.2855	0.065	0.62	0.80
E3	9.9 ± 0.6	96.6	0.1589	0.049	0.64	0.70
E4	7.6 ± 0.6	105.1	0.1739	0.049	0.68	0.72
E5	6.9 ± 0.6	127.4	0.2323	0.059	0.63	0.74

Fig. 5 shows the photoluminescence (PL) spectra of the prepared catalysts, indicating that they have similar curve shapes but different intensities.

The emission peak at 416 nm was due to the Wannier-Mott free exciton emission of TiO_2, whereas the peak at approximately 440 nm was due to a charge transfer transition from Ti^{3+} to the O_2^- in $[TiO_6]^{8-}$ (Chen et al., 2013). Additionally, the peaks at around 478 nm and 526 nm originated from oxygen vacancies and surface defects of TiO_2 (Klein et al., 2016). The lower PL intensity suggests a lower recombination of photogenerated electron-hole pairs, leading to an improved activity. As can be seen in Fig. 5, the catalysts with the lowest amount of nitrogen, such as E5 or E2, exhibited the lowest PL intensity. Conversely, the highest amount of nitrogen in the catalysts (10 % w/w) resulted in the strongest PL intensity, as observed for sample E3 and E1, which likely affects their catalytic activity.

3.2. Photocatalytic oxidation

The photocatalysis can be a promising technology for the PPCPs abatement using a suitable semiconductor, and its activity can be cheaper if solar radiation can be used as radiation source. In order to establish a good photoactivity under the visible spectrum a co-doping of TiO_2 was made. However, as observed in the previous section, the absorbance of the produced catalysts in the visible spectrum was not improved. In this sense, two different radiations sources were used: UVA and solar radiation. Fig. 6 presents the degradation of PCT by photocatalytic oxidation through

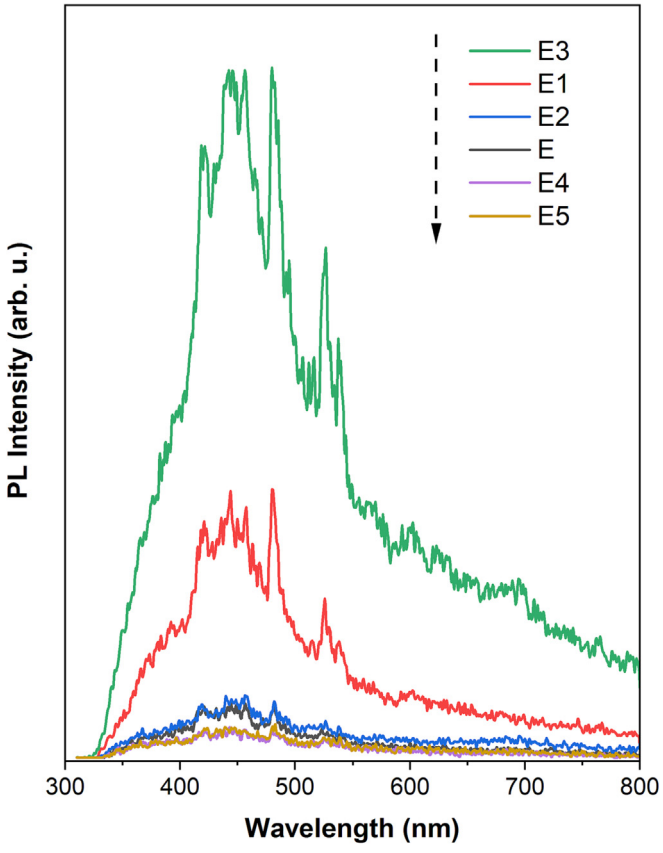

Fig. 5. Photoluminescence spectra of the prepared catalysts.

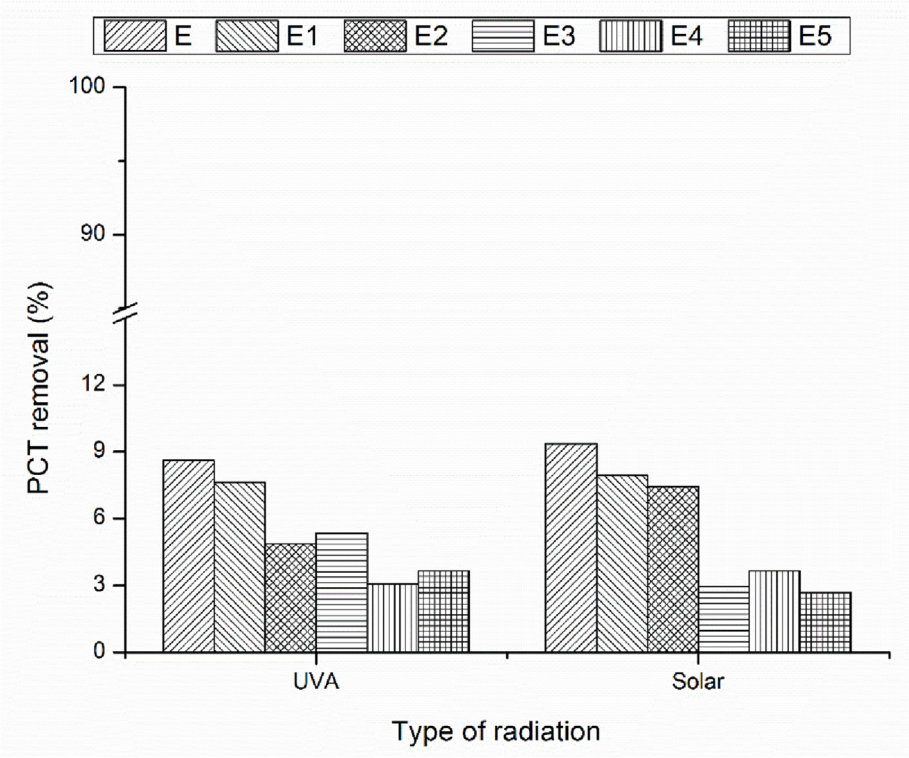

Fig. 6. Removal of paracetamol (PCT) following photocatalytic oxidation through UVA and solar radiation with the tested catalysts.

UVA and solar radiation. As abovementioned, the removal of PCT was similar to that of CBZ and SMX, whereas the removal of MP and PP was lower, with values between 2 and 8 %. Thus, the removal values for the PPCPs mixture are lower than the ones presented for PCT. Given this, the removal of PCT was presented to allow inferences about the effects of the N and Ce amount on co-doping TiO_2-based catalysts following photocatalytic oxidation. In a previous work of our group, the pristine TiO_2 presented a lower performance than N doped TiO_2 catalysts for degradation of a parabens mixture (Fernandes et al., 2020a) and, thus, it was not considered for this comparison between N and Ce doped TiO_2 catalysts.

The photolysis of different PPCPs for both radiations used did not promote any removal, since their absorption spectrum is out of this radiation wavelength (Martins et al., 2019; Gomes et al., 2021). In terms of catalysts performance, the PCT removal presented in Fig. 6 reveals the same type of response as other PPCPs used in the experiments. The PPCPs removal in the photocatalytic oxidation was slightly dependent on the radiation source used. The solar radiation presented a slightly better performance for PCT removal comparing to UVA radiation in the case of 0.6 % of Ce load (E, E1, E2 catalysts) but which is not significantly relevant. For the highest Ce load, the results were similar for both radiations used. As can be seen, the radiation source does not present significant differences as further obtained in data analysis section. The lowest Ce load promoted a higher PCT removal than the highest Ce load, which was unexpected. Actually, according to Fig. 1A, it was expected that the highest amount of Ce promoted a better removal since the slope of absorbance was less pronounced than that of the lowest Ce load. However, the increase of Ce ions in TiO_2 lattice can inhibit the anatase phase growth, decreasing the crystallite size (Sun et al., 2010). Based on a XRD analysis, Sun et al. (2010) reported that the increase of Ce load from 0.3 to 1.2 % caused a decrease in the crystallite size of anatase phase. Therefore, this explains the performance of both Ce loads used since the anatase phase is directly related with the photoactivity of catalysts (Pelaez et al., 2012; Gomes et al., 2019a). The results do not agree with the photoluminescence analysis (Fig. 5) which suggests that E5 has the lowest PL intensity. In this sense, it was expected that E5 had the lowest electron-hole pairs recombination and higher photocatalytic activity for the PCT degradation, which does not occur.

Regarding to the N load effect on the photocatalytic oxidation, results were more similar for both Ce loads (Fig. 6). Considering the lowest Ce amount, the increase of the N load from 2.5 (E2) to 5 % (E) promoted an improvement of PCT removal. However, a further increase in the N amount from 5 (E) to 10 % (E1) caused a decreased efficiency, achieving an optimal load of N at 5 %. These results indicate that the increase of the N amount can also affect the crystallite size and even inhibit the growth of anatase phase (Bu et al., 2012; Zielinska-Jurek et al., 2015; Gomes et al., 2019a). In fact, the calcination stage is when the amorphous phase transforms in anatase and this inhibition can contribute to the low crystallinity, ultimately reducing the efficiency on the PPCPs abatement. The presence of the amorphous phase, as shown by the XRD analysis (Fig. 2), sustains such low photocatalytic oxidation performance.

Despite this, the low performance observed for all the catalysts can be related with the low crystallinity since the 2 h of aging was not enough to obtain a Ti-O-Ti network with optimal physical and chemical properties (Chong and Jin, 2012). In further studies, the sol-gel procedure, in particular the aging time, should be optimized. Moreover, the catalyst dosage should also be optimized since other studies with higher amounts of catalyst presented better performance on PPCPs removal.

The mechanisms for the photocatalytic oxidation are described in Eq. (4) to Eq. (6) (Pelaez et al., 2012). This process encompasses the photoactivation of TiO_2-based catalysts through the UVA radiation promoting the photogeneration of electron-hole pairs (Eq. (4)). The photogenerated holes oxidize water to produce hydroxyl radicals (Eq. (5)) which presents the highest oxidative potential (2.80 V). On the other hand, the photogenerated electrons reduce the oxygen to produce superoxide radicals (Eq. (6)). Besides this, the low performance can be related with the low crystallinity of anatase phase due to the presence of amorphous phase as verified in the XRD analysis (Fig. 2).

$$TiO_2 + h\upsilon \rightarrow TiO_2(h^+) + TiO_2(e^-) \quad (4)$$

$$H_2O_{(ads)} + h^+ \rightarrow {}^{\bullet}OH + H^+ \quad (5)$$

$$O_{2(ads)} + e^- \rightarrow O_2^{\bullet-} \quad (6)$$

Table 3
Correlation matrix between the degradation of PCT and the loads of nitrogen and cerium in the prepared catalysts upon photocatalytic ozonation with solar radiation (sunlight).

$PCT_{removal}$	Nitrogen	Cerium	Solar radiation	
1	0.190	−0.868	0.031	$PCT_{removal}$
0.190	1	0	0	Nitrogen
−0.868	0	1	0	Cerium
0.031	0	0	1	Solar radiation

3.2.1. Data analysis

A more comprehensive data analysis was carried out covering the PCT removal presented in Fig. 6. A correlation analysis was done to understand the correlation between degradation of PCT, N load, Ce load and radiation source. Tables 3 and 4 present the correlation matrix between the PCT removal and the independent variables, load of nitrogen, load of cerium, UVA and solar radiation. The results of the correlation matrix corroborate the discussion presented in Section 3.2. The degradation of PCT is inversely correlated to the Ce load, having a high level of correlation (−0.868 and −0.867, respectively for solar and UVA radiation). The N load has a positive effect on the degradation of PCT, but it has a low level of correlation. Additionally, the UVA and solar radiation have almost no effect on the degradation of PCT (0.031 and −0.026, respectively).

Based on the results of degradation of PCT obtained for the different types of radiation and for the different catalysts, the results have been adjusted to further understand the significance of the dependence of the degradation of PCT on the type of radiation and catalysts. For this analysis, the solar radiation results were considered to be due to the slightly better correlation between the degradation of PCT and solar radiation (0.031, Table 3) instead of UVA radiation (−0.026, Table 3). The degradation of PCT can be treated as a linear regression with multiple variables following the equation (Eq. (7)):

$$PCT_{removal} = 10.816 + 0.143 \times \text{Nitrogen} - 6.807 \times \text{Cerium} + 0.144 \times \text{Solar} \quad (7)$$

However, the R^2 value (0.79) shows a low adjustment, which led to a further analysis to understand the correlation of degradation of PCT on the N amount in the catalysts. The results presented in Fig. 6 suggest that the different catalysts and solar radiation influence the degradation of PCT following the equation (Eq. (8)):

$$PCT_{removal} = 8.126 + 1.250 \times \text{Nitrogen} - 0.086 \times \text{Nitrogen}^2 - 6.807 \times \text{Cerium} + 0.144 \times \text{Solar} \quad (8)$$

A significant improvement in the adjustment was observed ($R^2 = 0.83$) indicating that most likely the influence of Nitrogen on the degradation of PCT is nonlinear, and suggesting a quadratic relationship between the degradation of PCT and the N amount.

Statistical significance analysis, building a model considering backward elimination, was applied to Eq. (8) to understand the overall influence and relationship between the different catalysts and radiation source on the degradation of PCT. Considering a statistical significance level of 0.05, the degradation of PCT expressed through Eq. (8) can be reduced to Eq. (9) ($R^2 = 0.83$):

$$PCT_{removal} = 8.198 + 1.250 \times \text{Nitrogen} - 0.086 \times \text{Nitrogen}^2 - 6.807 \times \text{Cerium} \quad (9)$$

The model proposed, Eq. (9), indicates that the degradation of PCT is not statistically dependent on the solar radiation used, as discussed in Section 3.2, as well as indicated in the correlation matrix (see Table 3). Also, the relationship between the degradation of PCT and the N and Ce loads in Eq. (9), are closed to the discussion presented in Section 3.2. The data analysis results through Eq. (9) can be an interesting contribution to the results presented in this work, indicating that the experimental results can be translated in terms of significant mathematical equations. Moreover, solving the Eq. (9) setting the partial derivative to Nitrogen equal to zero, gives a 7 % w/w of N as the optimal value to achieve the best degradation of PCT.

Table 4
Correlation matrix between the degradation of PCT and the loads of nitrogen and cerium in the prepared catalysts upon photocatalytic ozonation with UVA radiation.

$PCT_{removal}$	Nitrogen	Cerium	UVA radiation	
1	0.190	−0.867	−0.026	$PCT_{removal}$
0.190	1	0	0	Nitrogen
−0.867	0	1	0	Cerium
0.026	0	0	1	UVA radiation

3.2.2. Ecotoxicity evaluation for photocatalytic oxidation

In order to validate the treatment efficacy, besides following the PPCPs concentration for the different catalysts, ecotoxicological analysis was made on treated samples and compared to the initial synthetic solution of PPCPs. The ecotoxicological response of the model species upon exposure to the synthetic effluent treated by photocatalytic oxidation using the developed catalysts is presented in Fig. 7. The results of growth rate inhibition for *R. subcapitata* and L. *minor* are presented in Fig. S1 (Supplementary Material).

The microalgae *R. subcapitata* was very sensitive to the samples, exhibiting yield inhibition values above 85 % for all catalysts. Such high toxicity of the tested samples is likely related to the presence of the PPCPs, as suggested by the similar response to all treatments associated with the low PPCPs removal efficiency (Fig. 6). Indeed, a previous study also reported high yield inhibition of *R. subcapitata* exposed to a similar mixture of PPCPs (Jesus et al., 2022a). This pronounced response is likely related mainly to the presence of SMX given its toxicity to this microalga species, as literature EC50 values range from 0.146 to 4.74 mg/L (Jesus et al., 2022a). Compared to the SE, the treatments with the catalysts E2 and E4 caused lower inhibition ($F_{6,19} = 6.596$; $p = 0.002$). Interestingly, the catalyst E2, which caused the lower inhibition, was the one produced with the lowest N and Ce amounts (2.5 % and 0.6 %, respectively).

Regarding the yield inhibition of L. *minor,* based on the frond number, values for the treated samples ranged between 57 % (E5) and 69 % (E3), whereas SE caused a 32 % inhibition, underlying the existence of statistically significant differences between SE and the remaining treatments ($F_{6,20} = 39.814$; $p < 0.001$). These results suggest that the treated samples were more toxic than the untreated SE. The untreated mixture of PPCPs was also found to be toxic to this macrophyte in a previous study, with yield inhibition values about 65 % (Jesus et al., 2022a). As for the microalga, SMX is likely the main responsible for the observed toxicity, as EC50 values vary between 0.21 and 12.56 mg/L (Jesus et al., 2022a). The effects on the yield inhibition based on the dry weight were less pronounced varying between 11 % (E4) and 27 % (E2), with no significant differences among catalysts as well as between the SE and the treatments with the catalysts ($F_{6,20} = 1.510$; $p = 0.245$).

Daphnids showed a pronounced response after exposure to the samples treated with the catalysts E1 and E3, showing a 100 % immobilization, and less pronouncedly to E2 (60% immobilization). Compared to the SE, these differences were statistically significant for E1 and E3 ($H = 26.451$, $df = 6$, $p < 0.001$). In terms of PPCPs degradation, considering the example of PCT (Fig. 6), the catalysts E1 and E2 presented similar results while E3 showed a lower degradation. However, the daphnids response does not seem to be related with the PPCPs degradation, as the PPCPs were not toxic to the daphnids (immobilization of the untreated SE = 0 %). In fact, their response seems to be related to the composition of catalysts, as both E1 and E3 were produced with N at 10 %, which suggests the presence of some chemical compound toxic to the daphnids. One plausible explanation is

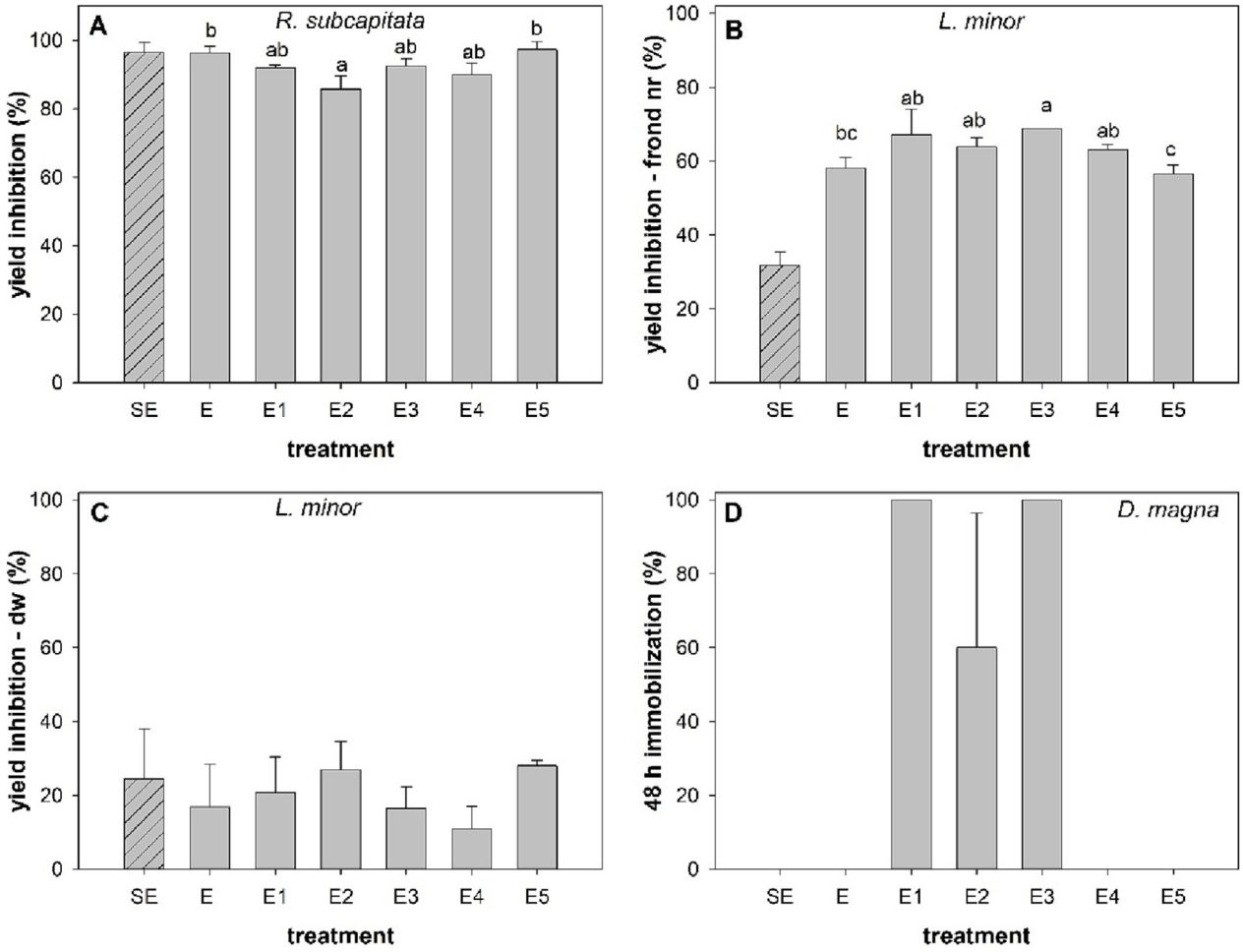

Fig. 7. Ecotoxicological response of the model species exposed to the synthetic effluent after treatment by photocatalytic oxidation using the tested catalysts: (A) Yield inhibition of *R. subcapitata* after 96 h of exposure; (B) yield inhibition (based on the frond number) of L. *minor* after 7 d of exposure; (C) yield inhibition (based on the dry weight) of *L. minor* after 7 d of exposure; (D) immobilization of *D. magna* after 48 h of exposure. Bars represent the mean and the error bars represent the standard deviation. Treatments sharing the same letter are not statistically different. SE – untreated synthetic effluent.

the production of toxic compounds deriving from urea, used as nitrogen precursor for N, during the calcination stage (Schaber et al., 2004). Indeed, the thermal decomposition of urea leads to the production of compounds such as cyanuric acid, ammelide and ammeline, which might persist at temperatures between 360 and 450 °C (Schaber et al., 2004). These compounds can leach to the reactional medium during the photocatalytic oxidation, as suggested by Fernandes et al. (2020a), promoting the daphnids immobilization. Interestingly, the same compounds were reported as degradation by-products of melamine under photocatalysis (UV light irradiation) in the presence of TiO_2 and H_2O_2, resulting in toxicity to *D. magna* (Bozzi et al., 2004), similarly to the results of the present study. Note that photocatalytic ozonation of a mixture of PPCPs with TiO_2 catalysts (no doping) caused no toxicity to *D. magna* (Gimeno et al., 2016), thus corroborating the above-mentioned hypothesis. Regarding the immobilization observed after exposure to the samples treated with the catalyst E2, this will require further investigation. A priori, the fact that this catalyst was produced with the lowest amount of both N and Ce among all catalysts, suggests that toxicity is unlikely due to leaching of any chemical from the catalyst. Thus, the most plausible explanation for the toxicity of the catalyst E2 is the formation of toxic by-products which were not further fully degraded.

Taken as a whole, the responses of the test species differed among species and, within each species, between the tested endpoints. This reflects the differing sensitivity of the species and must be taken into consideration when selecting an optimal catalyst or treatment. Catalysts represented an added-value only for the microalga; for the remaining species/endpoints the catalysts had no effect or a negative effect, compared to the untreated synthetic effluent. These results agree to the low efficiency of these catalysts on the PPCPs removal. Thus, under the used experimental conditions and an environmental safety perspective, the present results suggest that the tested catalysts have low interest to be applied in photocatalytic oxidation processes.

3.3. Photocatalytic ozonation

As shown in Fig. 6, the photocatalytic oxidation presented low efficiency on the abatement of PPCPs. However, the presence of ozone instead of air can improve the degradation of PPCPs by enhancing the production of radical species and even the ozone can work itself as an oxidant species (Kasprzyk-Hordern et al., 2003; Mehrjouei et al., 2015; Gimeno et al., 2016; Fernandes et al., 2020a). In fact, ozone is a highlly electrophilic species which can trap the electrons obtained from the photogenerated holes-electrons pairs, producing ozonide and hydroperoxyl radicals (Mehrjouei et al., 2015; Xiao et al., 2015). Besides this, the catalyst due to its specific surface area can enhance the ozone decomposition into radical species despite the low photoactivity under photocatalysis (Nawrocki, 2013; Gomes et al., 2018). This ozone decomposition into species with higher oxidative potential such as hydroxyl radicals (Kasprzyk-Hordern et al., 2003), translates into decreased amount of ozone required to achieve the same PPCP removal, and thus, reduced energy costs, with the evident economic and environmental benefits. Fig. 8 presents the PPCPs removal following photolytic and photocatalytic ozonation for the abatement of the PPCPs mixture as function of the transferred ozone dose (TOD). The photolytic ozonation consists in the combination of UVA radiation and ozone, using no catalysts.

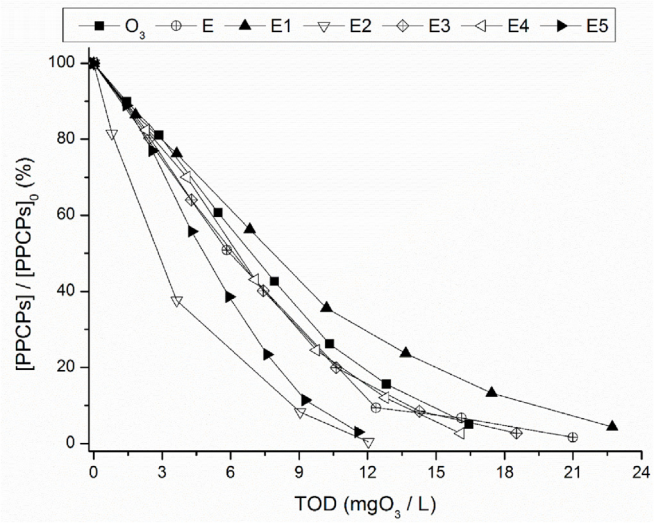

Fig. 8. PPCPs removal during photolytic (O_3) and photocatalytic ozonation through UVA radiation with the tested catalysts, as function of the transferred ozone dose (TOD). Results were obtained by dividing the sum of the concentration of the 5 PPCPs at the end of the reaction ([PPCPs]) by its initial concentration ($[PPCPs]_0$) and multiplying by 100 (percentage). Error bars were omitted for better readability-The standard error between replicates was <5 %.

The PPCPs abatement was followed for the mixture of 5 PPCPs during treatment with the different catalysts and ozone. The UVA was used as radiation source since the data analysis revealed no dependence on the radiation source.

The photolytic and photocatalytic ozonation were able to remove all the PPCPs almost completely. In fact, ozone presents a good performance over this mixture since the individual second order constant rates are in the range 2.5×10^5 and 2.6×10^6 M^{-1} s^{-1} (Huber et al., 2003; Tay et al., 2010; El Najjar et al., 2014). Moreover, Jesus et al. (2022b) verified, for the same mixture, that ozone was able to degrade all the five PPCPs even when spiked in secondary effluent. The catalysts coupled with ozone decreased the TOD amount required to achieve the complete removal of the PPCPs comparing to the photolytic ozonation. In particular, the catalysts with the lowest N amount (E2 and E5, both with 2.5 % N) presented the best performance over the PPCPs removal. On the other hand, the catalyst with the highest N load and the lowest Ce amount (E1) presented the worst result. In this sense, the lower N load is relevant for the decomposition of ozone into hydroxyl radicals and other radical species since reduced the ozone dose (Domenjoud et al., 2011; Yaghmaeian et al., 2017). Moreover, this result reveals that the photocatalytic activity of this catalyst is lower since the presence of more nitrogen should decrease the bandgap (Pelaez et al., 2012; Gomes et al., 2019a). In fact, the best ozone decomposition into hydroxyl radical species occurs with low N amount due to the lower crystallite size which presents a higher specific surface area (Dhanya and Sugunan, 2013; Solís et al., 2015). As can be seen in the Table 2, the best results was obtained for the higher surface area which increase the ozone decomposition reducing the TOD value to achieve the PPCPs complete removal. Fernandes et al. (2020a) verified for the sol-gel N-TiO_2 that the presence of more nitrogen means a decrease in the specific surface area and increase the crystallite size. On this way, the presence of radiation does not make any difference since these materials work as catalysts and not as photocatalysts.

Regarding to Ce, the impact is not so pronounced since the doping amount is lower compared to N. However, at the highest N load it is possible to observe its relevance. The increase in the Ce amount to 1.2 % on the 10 % of N (catalyst E3) allowed to achieve a TOD reduction for the PPCPs removal comparing with the Ce load of 0.6 % (catalyst E1). Qi et al. (2020) verified that the increase of Ce load on the catalytic ozonation of organic pollutants benefited the mineralization of wastewater. This was related with the availability of more active sites which promotes the ozone decomposition (Kasprzyk-Hordern et al., 2003). In this sense, it is important to find an equilibrium in the dopants load to achieve a good performance when doping is made. Moreover, in this case the photoactivity through UVA and/or visible radiation should be improved by the optimization of the sol-gel procedure. The pronounced reduction in the TOD observed for the catalysts E2 and E5 compared to photolytic ozonation suggests an opportunity to reduce the operational costs of wastewater treatment under real conditions. The presence of the E2 catalyst decreased the TOD values to half compared to single ozonation (Jesus et al., 2022a) to achieve the PPCPs complete removal. Considering that ozone production is the main cost in the ozonation process, the use of this catalyst (E2) roughly reduces this cost to half. Regarding the catalyst costs, they will be minimal since a low amount was used (100 mg/L) and the catalyst can be reused after a suitable separation from the aqueous matrix, like sedimentation. However, further studies should be made in order to evaluate the stability and reusability of these catalysts.

In the ozonation based processes instead of time it is important to consider the ozone consumed for the PPCPs removal (Domenjoud et al., 2011), and in this sense is important to compare the TOD and time. The pseudo-first order kinetic model was used as a function of time or as a function of TOD (Eqs. (10) and (11), respectively) (Gomes et al., 2022).

$$C/C_0 = e^{-k't} \quad (10)$$

$$C/C_0 = e^{-k'TOD} \quad (11)$$

In Eqs. (10)–(11), C_0 and C represent the PPCP concentration before the photocatalytic ozonation reaction (time zero) and during reaction, respectively; k' is the pseudo-first order kinetic rate constant which was determined from the mixture of 5 PPCPs degradation profile in terms of time (k't) and in terms of TOD (k'TOD). The pseudo-first order kinetic rate constants calculated from our results in terms of TOD and time values are presented in Table 5.

According to Table 5, the pseudo-first order kinetic rates present very different results among the catalysts when TOD was considered, although this is not the case for time. In fact, the reaction time was almost the same for all the catalysts which turns the results very similar. The difference is likely related to the ozone transferred to the reactional media. Considering TOD, it is possible to see that E2, E5 and E, by this order, are better than the photolytic ozonation. Moreover, in the case of E2, this difference almost doubled, which can mean a significant reduction of ozone dose to achieve the complete removal of PPCPs. Therefore, the E2 catalyst can be a suitable option for the treatment of PPCPs with low consumption of ozone.

In the photocatalytic ozonation, the hydroxyl radical production can occur by two different ways: ozone decomposition at the catalyst surface by catalytic reaction or even due to the water oxidation by photogenerated hole pairs (Eq. (5)) (Pelaez et al., 2012; Mehrjouei et al., 2015). Otherwise, this radiation could not break the ozone into hydroxyl radicals, since the molecular ozone adsorption edge is about 254 nm. On the other hand, according Eq. (12) the photogenerated electrons can reduce the ozone into ozonide radicals (O_3^{-}•) which present low oxidative potential compared to

Table 5
Pseudo-first order kinetic rate constants of photocatalytic ozonation for different catalysts and single ozone, as a function of time (k') and as a function of TOD (k'_{TOD}), with the corresponding adjusted coefficients of determination (adj R^2).

	O_3	E	E1	E2	E3	E4	E5
k'_{TOD} (mg O_3^{-1}) (adj R^2)	0.125 (0.980)	0.149 (0.976)	0.104 (0.985)	0.276 (0.998)	0.139 (0.974)	0.138 (0.960)	0.183 (0.950)
k' (min^{-1}) (adj R^2)	0.082 (0.973)	0.114 (0.965)	0.090 (0.984)	0.122 (0.930)	0.130 (0.989)	0.118 (0.983)	0.091 (0.978)

hydroxyl radicals (Mehrjouei et al., 2015). Moreover, in the presence of acidic medium the ozonide radicals can be converted into hydroxyl radicals (Eq. (13)). Hence, the oxidation mechanism for the PPCPs mixture degradation can be through hydroxyl and/or ozonide radicals, as well as through the molecular ozone activity. However, the mechanistic study underlying the PPCPs degradation must be explored in further works.

$$O_{3(ads)} + e^- \rightarrow O_3^{\bullet-} \quad (12)$$

$$O_3^{\bullet-} + H^+ \rightarrow HO^{\bullet}{}_3 \rightarrow {}^{\bullet}OH + O_2 \quad (13)$$

3.3.1. Ecotoxicity evaluation for photocatalytic ozonation

The ecotoxicological response of the biological species following exposure to the synthetic effluent treated by photocatalytic ozonation with UVA is presented in Fig. 9. The results of the growth rate inhibition for *R. subcapitata* and L. *minor* are presented in Fig. S2 (Supplementary Material).

For the microalga, the yield inhibition caused by the photocatalytic ozonation with the catalysts varied between 44 % (E2) and 68 % (E5). These values are similar to the one obtained for single ozonation (60 % inhibition). No differences among the treatments with the catalysts were found, despite a slight trend for the catalysts with the highest Ce amount (E3, E4 and E5) to cause higher toxicity than those with the lowest amount (E, E1 and E2). The very low toxicity of the catalyts E3, E4 and E5 during photocatalysis suggests that the trend observed during photocatalytic ozonation will likely be due to the formation of toxic by-products related to the higher Ce amount in the catalysts and, possibly, in the reactional medium owing to leaching from the catalysts. This is corroborated by a low toxicity of Ce to this microlagae species (EC50 = 1.6 mg /L, and EC10 = 0.5 mg/L, for the endpoint 72 h-growth inhibition) (Siciliano et al., 2021). Moreover, no significant differences between the photocatalytic ozonation treatments and the photolytic ozonation treatment were found, suggesting a minor contribution of the catalysts in the treatment of the samples. However, compared to the untreated SE (96 % inhibition), the treatments with catalysts E1, E2 and E4, as well as photolytic ozonation (O_3), showed lower toxicity ($F_{6,20} = 3.954$; $p = 0.016$), which highlights that these treatments were effective in reducing the toxicity of the PPCPs mixture to this micoalgae species. Noticeably, compared to the photocatalytic treatments, a lower toxicity was achieved, which highlights the benefits of combining both oxidation treatments (photocatalysis and ozonation).

The response of the macrophyte differed according to the endpoint. Considering the yield inhibition based on the frond number (Fig. 9B), the treatment with the catalysts promoted a pronounced toxicity decrease compared to the untreated SE (range − 3 % to 13 %, and 49 %, respectively), statistically significant for all treatments ($F_{7,23} = 14.752$; $p < 0.001$). A previous study also reported that photocatalytic ozonation of a mixute of parabens, using a 10 % N-doped TiO_2 catalyst promoted the germination of the water cress *Lepidium sativum* (Fernandes et al., 2020b), also a primary producer, such as the macrophyte and the microalgae. The results of the previously mentioned study thus agree with our results regarding both the microalgae and the macrophyte for the endpoint yield inbibition based on the frond number. The fact that the values obtained by photocatalytic ozonation are similar to the treatment by photolytic ozonation (1 %)

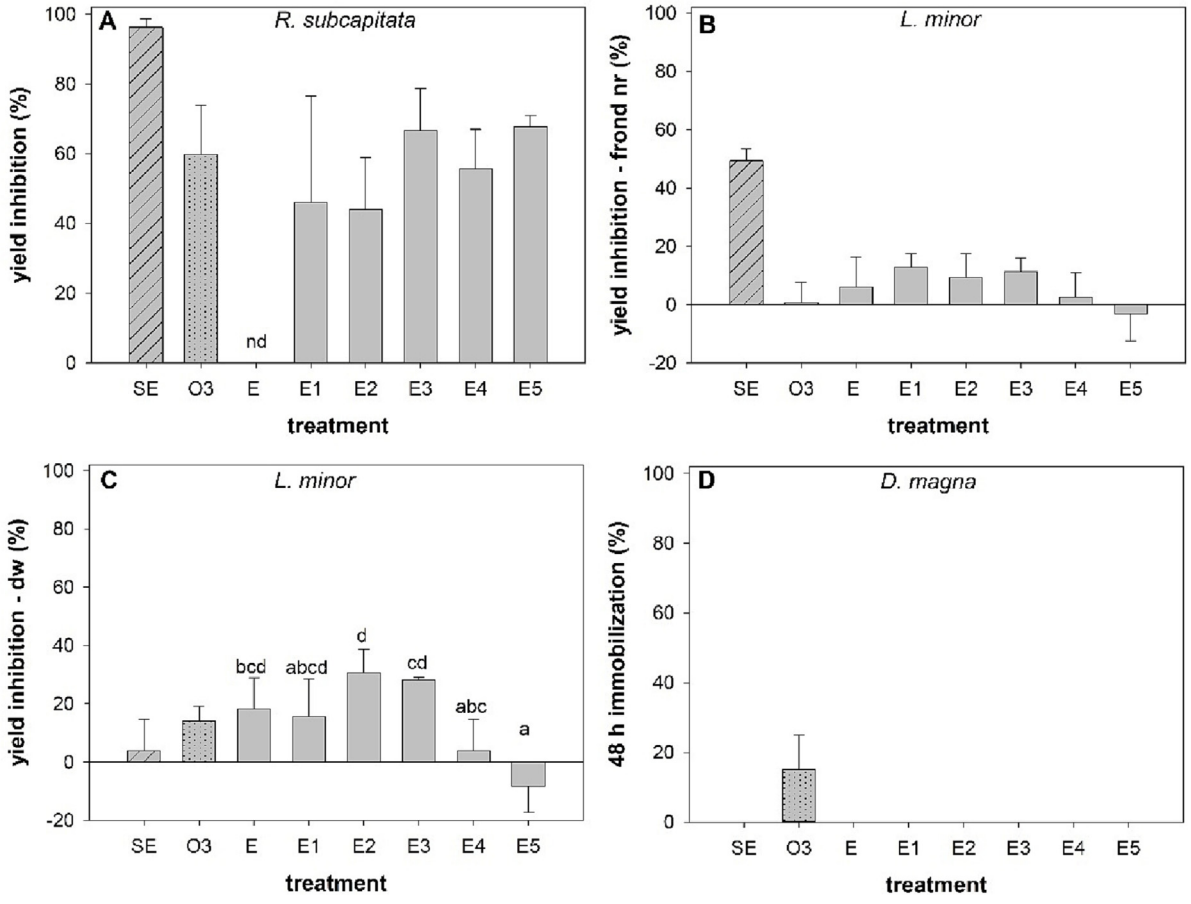

Fig. 9. Ecotoxicological response of the model species exposed to the synthetic effluent after treatment by photocatalytic ozonation using the tested catalysts: (A) Yield inhibition of *R. subcapitata* after 96 h of exposure; (B) yield inhibition (based on the frond number) of L. *minor* after 7 d of exposure; (C) yield inhibition (based on the dry weight) of *L. minor* after 7 d of exposure; (D) immobilization of *D. magna* after 48 h of exposure. Bars represent the mean and the error bars represent the standard deviation. Treatments sharing the same letter are not statistically different. SE – untreated synthetic effluent; O3 – SE after treatment by photolytic ozonation; nd – not determined.

suggests that catalysts represented no added-value to the ozonation treatment, as also observed for the microalga. Regarding the yield inhibition based on the dry weight (Fig. 9C), there were significant differences among treatments, with the catalyst E5 promoting increased dry weight compared to catalysts E, E2 and E3. Compared to the photolytic ozonation treatment, only this catalyst (E5) led to statistically significant differences ($F_{7,23}$ = 6.040; p = 0.001), highlighting an improvement of the water treatment process. The high Ce amount used in the production of the catalyst E5 (2.5 % N, 1.2 % Ce) allied to ozone can favor the production of hydroxyl radicals (Qi et al., 2020) which can lead to higher degradation of the toxic by-products and, ultimately, to lower toxicity, making this the most favourable catalyst for the L. *minor* species. It is noteworthy to mention that photolytic ozonation led to a slight increase in the toxicity of the sample (despite not statistically significant), and only the treatment with the catalyst E5 was able to reduce that toxicity to a value even lower than that of the untreated SE. The toxicity increment caused by photolytic ozonation might be related to the formation of toxic degradation by-products, and agrees with the increased toxicity observed after ozonation of a similar mixture in a previous study (Jesus et al., 2022a) and after oxidation processes of some of the tested PPCPs individually (e.g., Gómez-Ramos et al., 2011; Oropesa et al., 2017). Compared to the untreated SE, the treatments with the catalysts E2 and E3 showed an undisered effect by increasing toxicity to this species. Since these catalysts do not share the N and Ce amounts used in their production, the observed toxicity might be due to the formation of toxic by-products, rather than to their chemical composition per se. It is worth to mention that, compared to the photocatalytic treatments, a lower toxicity was achieved in the photocatalytic ozonation treatments regarding the endpoint yield based on the frond number, but an increase regarding the endpoint yield based on dry weight. As previously mentioned, the same species can exhibit different responses for different endpoints.

For the crustacean *D. magna* only the treatment of single ozonation caused toxicity (15 % immobilization). A previous study reported a very similar immobilization value (12 %) after exposure to a similar mixture (Jesus et al., 2022a), likely motivated by formation of toxic ozonation-by products. The lack of toxicity of the samples treated by photocatalytic ozonation with the developed catalysts, compared to the photolytic ozonation, suggests that for this species, the catalysts represented an added value, decreasing toxicity. This is particularly notorious considering that the catalysts E1, E2 and E3, used in the photocatalytic treatments (Fig. 7) caused a very pronounced immobilization (60–100 %). This suggests that the toxic compounds responsible for the immobilization were degraded owing to the action of ozone and hydroxyl radicals.

Overall, the ecotoxicological data show a benefitial effect of using photocatalytic ozonation instead of single photocatalysis, also observed for the ecotoxicity expressed as growth rates inhibition (Figs. S1 and S2 in Supplementary Material). This trend was also observed in several studies with TiO_2 catalysts, for various contaminants (e.g., Santiago-Morales et al., 2012; Solís et al., 2016). Previous studies report that photocatalytic ozonation commonly decreased effluent toxicity while accomplishing a high removal of the target contaminants (see review by Lashuk and Yargeau, 2021). In the present study, a benefitial effect of using photocatalytic ozonation rather than single photolytic ozonation was observed only for *L. minor* (endpoint yield based on dry weight) and for *D. magna*, as for the other species the use of the tested catalysts represented no added-value. Based on these results, the catalyst E5, prepared by co-doping TiO_2 with 2.5 % w/w N and 1.2 % w/w Ce, showed to be the most promising catalyst, among the tested catalysts. Interestingly, this catalyst, together with E2, presented the best performance over the PPCPs removal (Fig. 8). However, we suggest that future studies encompass a wider diversity of species, aiming to gain a comprehensive overview on the potential benefits of combining photocatalysis with ozonation and to select the catalyst achieving the best ecotoxicological performance. Moreover, future studies should also consider using raw wastewater as the aqueous matrix, as this represents a more realistic condition. The results indicate that the use of TiO_2 catalysts co-doped with Ce and N in a real wastewater will contribute to improve PPCPs removal through photocatalytic ozonation.

4. Conclusions

The development of photocatalysts to be used with higher efficiency under visible light is a challenge to the scientific community. In this work, TiO_2-based photocatalysts were produced using nitrogen and cerium (at different weight ratios) as co-dopants, owing to their interesting characteristics for this purpose. However, due to the applied sol-gel procedure the catalysts revealed low efficiency for abatement of the mixture of PPCPs under photocatalysis with solar and UVA radiation after 2 h of irradiation (below 20 % of removal). For this reason, further studies should address the optimization of the sol-gel procedure. Despite the data analysis to the N load indicated that the optimal load in the photocatalytic oxidation treatment should be 7 % w/w, the ecotoxicological data showed that high N load was toxic to *D. magna,* likely related to the products obtained during the calcination stage of urea, the nitrogen percursor. Therefore, to overcome this drawback, the calcination phase should be extended during the catalyst preparation procedure. Moreover, in general, the tested catalysts showed no or low added-value for reducing the toxicity of the synthetic effluent through photocatalytic oxidation.

Despite the low efficiency through photocatalysis, some catalysts, mainly the ones with lower N amount (catalysts E2 and E5), presented a good performance using photocatalytic ozonation reducing the TOD required for the complete removal of PPCPs comparing to photolytic ozonation. Moreover, the catalyst E5 was able to decrease the ecotoxicological impact of the synthetic effluent compared to photolytic ozonation for L. *minor* (endpoint yield based on dry weight) and for *D. magna*, thus representing an added-value. Still, it is worth to mention that the tested catalysts represented no added-value for the remaining species/endpoints. Hence, regarding its application in photocatalytic ozonation, E5 (prepared by co-doping TiO_2 with 2.5 % w/w N and 1.2 % w/w Ce) is suggested as the most promising catalyst, among the tested ones. The developed catalyst can be applied coupled with ozone in a slurry reactor system with environmental and economic benefits for the PPCPs abatement in urban wastewater. Moreover, to improve the removal performance, a compound parabolic collector (CPC) can be applied on the reactor to enhance the sunlight absorption, further contributing to decrease the ozone consumption. However, additional studies are required to assess the relationship cost-benefit of this additional feature in terms of degradation yield and toxicity reduction. Notwithstanding the interest of the tested catalysts for photocatalytic ozonation processes, future studies must be carried out aiming to further optimize the N:Ce ratio to achieve improved results considering their ecotoxicological impact, in addition to their efficiency in the removal of the target compounds.

CRediT authorship contribution statement

Eva Domingues: Writing - original draft preparation; Data curation; Investigation; Conceptualization; Methodology; Fátima Jesus: Writing - original draft preparation; Data curation; Investigation; Conceptualization; Mariana Alvim: Data curation; Investigation; Carla Cotas: Data curation; Writing - original draft preparation; Pawel Mazierski: Data curation; Investigation; Methodology; Writing - review and editing; Joana L. Pereira: Writing - review and editing; Funding acquisition; Supervision. João Gomes: Conceptualization; Writing - review and editing; Funding acquisition; Supervision; Methodology.

Data availability

The authors do not have permission to share data.

Declaration of competing interest

The authors declare that they have no known competing financial interests or personal relationships that could have appeared to influence the work reported in this paper.

Acknowledgments

This work was financially supported by Fundação para a Ciência e Tecnologia (FCT-MCTES), Portugal, under contract UIDB/00102/2020. The authors would like to acknowledge FCT for the financial support to João Gomes (CEECIND/01207/2018) and Eva Domingues for the PhD Grant (SFRH/BD/144096/2019). Thanks are due to FCT/MCTES for the financial support to CESAM (UIDP/50017/2020 + UIDB/50017/2020 + LA/P/0094/2020) through national funds.

Appendix A. Supplementary data

Supplementary data to this article can be found online at https://doi.org/10.1016/j.scitotenv.2023.164000.

References

Ahmed, M.B., Zhou, J.L., Ngo, H.H., Guo, W., Thomaidis, N.S., Xu, J., 2017. Progress in the biological and chemical treatment technologies for emerging contaminant removal from wastewater: a critical review. J. Hazard. Mater. 323, 274–298.

ASTM, 2004. Standard guide for conducting daphnia magna life-cycle toxicity tests. ASTM E1193 - 97(2004). American Society for Testing and Materials, Pennsylvania.

Bozzi, A., Dhananjeyan, M., Guasaquillo, I., Parra, S., Pulgarin, C., Weins, C., Kiwi, J., 2004. Evolution of toxicity during melamine photocatalysis with TiO_2 suspensions. J. Photochem. Photobiol. A Chem. 162, 179–185.

Bu, X., Zhang, G., Zhang, C., 2012. Effect of nitrogen doping on anatase–rutile phase transformation of TiO_2. Appl. Surf. Sci. 258, 7997–8001.

Centi, G., Perathoner, S., 2014. Advanced oxidation processes in water treatment. In: Duprez, D., Cavani, F. (Eds.), Handbook of Advanced Methods and Processes in Oxidation Catalysis. Imperial College Press, London, pp. 251–283.

Charanpahari, A., Umare, S.S., Sasikala, R., 2013. Effect of Ce, N and S multi-doping on the photocatalytic activity of TiO_2. Appl. Surf. Sci. 282, 408–414.

Chen, K., Feng, X., Hu, R., Li, Y., Xie, K., Li, Y., Gu, H., 2013. Effect of ag nanoparticle size on the photoelectrochemical properties of ag decorated TiO_2 nanotube arrays. J. Alloys Compd. 554, 72–79.

Chong, M.N., Jin, B., 2012. Sol-gel Synthesis of inorganic mesostructured composite photocatalyst for water purification: an insight into the synthesis fundamentals, reaction, and binding mechanisms. Synth. React. Inorg., Met.-Org., Nano-Met. Chem. 42 (1), 68–75.

Cvetnic, M., Juretic Perisic, D., Kovacic, M., Ukic, S., Bolanca, T., Rasulev, B., Kusic, H., Loncaric Bozic, A., 2019. Toxicity of aromatic pollutants and photooxidative intermediates in water: a QSAR study. Ecotoxicol. Environ. Saf. 169, 918–927.

Dhanya, T.P., Sugunan, S., 2013. Preparation, characterization and photocatalytic activity of N doped TiO_2. J. Appl. Chem. 4, 27–33.

Ding, W., Li, W., 2015. A first principles study of the energetics and core level shifts of anion-doped TiO2 photocatalysts. Chin. J. Catal. 36, 181–187.

Domenjoud, B., Tatari, C., Esplugas, S., Baig, S., 2011. Ozone-based processes applied to municipal secondary effluents. Ozone Sci. Eng. 33, 243–249.

Eggen, R.I.L., Hollender, J., Joss, A., Schärer, M., Stamm, C., 2014. Reducing the discharge of micropollutants in the aquatic environment: the benefits of upgrading wastewater treatment plants. Environ. Sci. Technol. 48 (14), 7683–7689.

El Najjar, N.H., Touffet, A., Deborde, M., Journel, R., Leitner, N.K.V., 2014. Kinetics of paracetamol oxidation by ozone and hydroxyl radicals, formation of transformation products and toxicity. Sep. Purif. Technol 136, 137–143.

Fan, Z., Meng, F., Gong, J., Li, H., Ding, Z., Ding, B., 2016. One-step hydrothermal synthesis of mesoporous Ce-doped anatase TiO2 nanoparticles with enhanced photocatalytic activity. J. Mater. Sci. Mater. Electron. 27, 11866–11872.

Fernandes, E., Contreras, S., Medina, F., Martins, R.C., Gomes, J., 2020a. N-doped titanium dioxide for mixture of parabens degradation based on ozone action and toxicity evaluation: precursor of nitrogen and titanium effect. Process Saf. Environ. Prot. 138, 80–89.

Fernandes, E., Martins, R.C., Gomes, J., 2020b. Photocatalytic ozonation of parabens mixture using 10% N-TiO_2 and the effect of water matrix. Sci. Total Environ. 718, 137321.

Gimeno, O., García-Araya, J.F., Beltrán, F.J., Rivas, F.J., Espejo, A., 2016. Removal of emerging contaminants from a primary effluent of municipal wastewater by means of sequential biological degradation-solar photocatalytic oxidation processes. Chem. Eng. J. 290, 12–20.

Gomes, J., Costa, R., Quinta-Ferreira, R.M., Martins, R.C., 2017. Application of ozonation for pharmaceuticals and personal care products removal from water (review). Sci. Total Environ. 586, 265–283.

Gomes, J.F., Quinta-Ferreira, M.E., Costa, R., Quinta-Ferreira, R.M., Martins, R.C., 2018. Paraben degradation using catalytic ozonation over volcanic rocks. Environ. Sci. Pollut. Res. 25, 7346–7357.

Gomes, J.F., Lincho, J., Domingues, E., Quinta-Ferreira, R.M., Martins, R.C., 2019a. N-TiO_2 photocatalysts: photocatalysts: a review of their characteristics and capacity for emerging contaminants removal. Water 11 (2).

Gomes, J.F., Frasson, D., Pereira, J.L., Gonçalves, F.J.M., Castro, L.M., Quinta-Ferreira, R.M., Martins, R.C., 2019b. Ecotoxicity variation through parabens degradation by single and catalytic ozonation using volcanic rock. Chem. Eng. J. 360, 30–37.

Gomes, J., Jesus, F., Domingues, E., Gonçalves, F., Pereira, J.L., Martins, R.C., 2021. Photocatalytic oxidation of pharmaceutical contaminants of emerging concern using sunlight and visible radiation: mechanism and ecotoxicological evaluation. J. Water Process. Eng. 43, 102204.

Gomes, J., Jesus, F., Bernardo .F., C., Pereira, J.L., Martins, R.C., 2022. Ozone kinetic studies assessment for the PPCPs abatement: mixtures relevance. ChemEngineering. 6, 20.

Gómez-Ramos, M.M., Mezcua, M., Agüera, A., Fernández-Alba, A.R., Gonzalo, S., Rodríguez, A., Rosal, R., 2011. Chemical and toxicological evolution of the antibiotic sulfamethoxazole under ozone treatment in water solution. J. Hazard. Mater. 192, 18–25.

Huber, M.M., Canonica, S., Park, G.-Y., Von Gunten, U., 2003. Oxidation of pharmaceuticals during ozonation and advanced oxidation processes. Environ. Sci. Technol. 37, 1016–1024.

Jesus, F., Bernardo, C., Martins, R.C., Gomes, J., Pereira, J.L., 2022a. Ecotoxicological consequences of the abatement of contaminants of emerging concern by ozonation: does mixture complexity matter? Water. 14 (11), 1801.

Jesus, F., Domingues, E., Bernardo, C., Pereira, J.L., Martins, R.C., Gomes, J., 2022b. Ozonation of selected pharmaceutical and personal care products in secondary effluent—degradation kinetics and environmental assessment. Toxics. 10 (12), 765.

Kalantari, K., Kalbasi, M., Sohrabi, M., Javid, S., 2016. Synthesis and characterization of N-doped TiO_2 nanoparticles and their application in photocatalytic oxidation of dibenzothiophene under visible light. Ceram. Int. 42, 14834–14842.

Kasprzyk-Hordern, B., Ziółek, M., Nawrocki, J., 2003. Catalytic ozonation and methods of enhancing molecular ozone reactions in water treatment. Appl. Catal. B Environ. 46 (4), 639–669.

Klein, M., Nadolna, J., Gołąbiewska, A., Mazierski, P., Klimczuk, T., Remita, H., Zaleska-Medynska, A., 2016. The effect of metal cluster deposition route on structure and photocatalytic activity of mono- and bimetallic nanoparticles supported on TiO_2 by radiolytic method. Appl. Surf. Sci. 378, 37–48.

Lashuk, B., Yargeau, V., 2021. A review of ecotoxicity reduction in contaminated waters by heterogeneous photocatalytic ozonation. Sci. Total Environ. 787, 147645.

Lee, H.U., Lee, S.C., Choi, S., Son, B., Lee, S.M., Kim, H.J., Lee, J., 2013. Efficient visible-light induced photocatalysis on nanoporous nitrogen-doped titanium dioxide catalysts. Chem. Eng. J. 228, 756–764.

Lincho, J., Gomes, J., Martins, R.C., 2021. Paraben compounds—part II: an overview of advanced oxidation processes for their degradation. Appl. Sci. 11 (8), 3556.

Martins, R.C., Domingues, E., Bosio, M., Quina, M.J., Gmurek, M., Quinta-Ferreira, R.M., Gomes, J., 2019. Effect of different radiation sources and noble metal doped onto TiO_2 for contaminants of emerging concern removal. Water. 11, 894.

Mehrjouei, M., Müller, S., Möller, D., 2015. A review on photocatalytic ozonation used for the treatment of water and wastewater. Chem. Eng. J. 263, 209–219.

Nawrocki, J., 2013. Catalytic ozonation in water: controversies and questions. Discussion paper. Appl. Catal. B 142–143, 465–471.

OECD, 2004. Test N202: Daphnia sp., Acute Immobilisation Test. OECD Guidelines for the Testing of Chemicals. Organisation for Economic Co-operation and Development, Paris, p. 12.

OECD, 2006. Test N221: Lemna sp. Growth Inhibition Test. OECD Guidelines for the Testing of Chemicals. Organisation for Economic Co-operation and Development, Paris, p. 22.

OECD, 2011. Test N201: Freshwater Alga and Cyanobacteria, Growth Inhibition Test. OECD Guidelines for the Testing of Chemicals. Organisation for Economic Co-operation and Development, Paris, p. 25.

O'Regan, B., Gratzel, M., 1991. A low cost high efficiency solar cell based on dye sensitized colloidal TiO_2 films. Nature. 353, 737–740.

Oropesa, A.L., Beltrán, F.J., Floro, A.M., Sagasti, J.J.P., Palma, P., 2017. Ecotoxicological efficiency of advanced ozonation processes with TiO_2 and black light used in the degradation of carbamazepine. Environ. Sci. Pollut. Res. 25, 1670–1682.

Pelaez, M., Nolan, N.T., Pillai, S.C., Seery, M.K., Falaras, P., Kontos, A.G., Dunlop, P.S.M., Hamilton, J.W.J., Byrne, J.A., O'Shea, K., Entezari, M.H., Dionysiou, D.D., 2012. A review on the visible light active titanium dioxide photocatalysts for environmental applications. Appl. Catal. B Environ. 125, 331–349.

Petala, A., Frontistis, Z., Antonopoulou, M., Konstantinou, I., Kondarides, D.I., Mantzavinos, D., 2015. Kinetics of ethyl paraben degradation by simulated solar radiation in the presence of N-doped TiO_2 catalysts. Water Res. 81, 157–166.

Pham, T.D., Lee, B.K., 2017. Selective removal of polar VOCs by novel photocatalytic activity of metals co-doped TiO_2/PU under visible light. Chem. Eng. J. 307, 63–73.

Qi, W., Wang, J., Quan, X., Chen, S., Yu, H., 2020. Catalytic ozonation by manganese, iron and cerium oxides on γ-Al2O3 pellets for the degradation of organic pollutants in continuous fixed-bed reactor. Ozone Sci. Eng. 42 (2), 136–145.

Qiu, P., Sun, X., Lai, Y., Gao, P., Chen, C., Ge, L., 2019. N-doped TiO_2@TiO_2 visible light active film with stable and efficient photocathodic protection performance. J. Electroanal. Chem. 844, 91–98.

Rimoldi, L., Pargoletti, E., Meroni, D., Falletta, E., Cerrato, G., Turco, F., Cappelletti, G., 2018. Concurrent role of metal (Sn, Zn) and N species in enhancing the photocatalytic activity of TiO_2 under solar light. Catal. Today 313, 40–46.

Rizzo, L., Malato, S., Antakyali, D., Beretsou, V.G., Đolić, M.B., Gernjak, W., Heath, E., Ivancev-Tumbas, I., Karaolia, P., Ribeiro, A.R.L., Mascolo, G., McArdell, C., Schaar, H., Silva, A.M.T., Fatta-Kassinos, D., 2019. Consolidated vs new advanced treatment methods for the removal of contaminants of emerging concern from urban wastewater. Sci. Total Environ. 655, 986–1008.

Rodriguez-Narvaez, O.M., Peralta-Hernandez, J.M., Goonetilleke, A., Bandala, E.R., 2017. Treatment technologies for emerging contaminants in water: a review. Chem. Eng. J. 323, 361–380.

Salimi, M., Esrafili, A., Gholami, M., Jonidi Jafari, A., Rezaei Kalantary, R., Farzadkia, M., Kermani, M., Sobhi, H.R., 2017. Contaminants of emerging concern: a review of new approach in AOP technologies. Environ. Monit. Assess. 189 (8).

Santiago-Morales, J., Gómez, M.J., Herrera, S., Fernández-Alba, A.R., García-Calvo, E., Rosal, R., 2012. Oxidative and photochemical processes for the removal of galaxolide and tonalide from wastewater. Water Res. 46, 4435–4447.

Schaber, P.M., Colson, J., Higgins, J., Thielen, D., Anspach, B., Brauer, J., 2004. Thermal decomposition (pyrolysis) of urea in an open reaction vessel. Thermochim. Acta 424, 131–142.

Shen, X.-Z., Liu, Z.-C., Xie, S.-M., Guo, J., 2009. Degradation of nitrobenzene using titania photocatalyst co-doped with nitrogen and cerium under visible light illumination. J. Hazard. Mater. 162, 1193–1198.

Shkir, M., Yahia, V.G.I.S., 2018. Microwave-synthesis of La^{3+} doped PbI_2 nanosheets (NSs) and their characterizations for optoelectronic applications. J. Mater. Sci. Mater. Electron. 29, 15838–15846.

Siciliano, A., Guida, M., Serafini, S., Micillo, M., Galdiero, E., Carfagna, S., Salbitani, G., Tomassi, F., Lofrano, G., Suarez, E.G.P., Gjata, I., Brouziotis, A.A., Trifuoggi, M., Liguori, R., Race, M., Fabbricino, M., Libralato, G., 2021. Long-term multi-endpoint exposure of the microalga Raphidocelis subcapitata to lanthanum and cerium. Sci. Total Environ. 790, 148229.

Solís, R.R., Javier Rivas, F., Gimeno, O., Pérez-Bote, J.L., 2015. Photocatalytic ozonation of pyridine-based herbicides by N-doped titania. J. Chem. Technol. Biotechnol. 91, 1998–2008.

Solís, R.R., Javier Rivas, F., Martínez-Piernas, A., Agüera, A., 2016. Ozonation, photocatalysis and photocatalytic ozonation of diuron. Intermediates identification. Chem. Eng. J 292, 72–81.

Stein, J.R., 1979. Handbook of phycological methods: culture methods and growth measurements. Vol. 1 CUP archive.

Sun, X., Liu, H., Dong, J., Wei, J., Zhang, Y., 2010. Preparation and characterization of Ce/N-Codoped TiO_2 particles for production of H_2 by photocatalytic splitting water under visible light. Catal. Lett. 135, 219–225.

Taheran, M., Naghdi, M., Brar, S.K., Verma, M., Surampalli, R.Y., 2018. Emerging contaminants: here today, there tomorrow! Environ. Nanotechnol. Monit. Manag. 10, 122–126.

Tay, K.S., Rahman, N.A., Abas, M.R.B., 2010. Ozonation of parabens in aqueous solution: kinetics and mechanism of degradation. Chemosphere. 81, 1446–1453.

Touati, A., Hammedi, T., Najjar, W., Ksibi, Z., Sayadi, S., 2016. Photocatalytic degradation of textile wastewater in presence of hydrogen peroxide: effect of cerium doping titania. J. Ind. Eng. Chem. 35, 36–44.

Velegraki, T., Hapeshi, E., Fatta-Kassinos, D., Poulios, I., 2015. Solar-induced heterogeneous photocatalytic degradation of methyl-paraben. Appl. Catal. B Environ. 178, 2–11.

Walker, C., 2014. Ecotoxicology. Effects of Pollutants on the Natural Environment. CRC Press, Taylor & Francis Group, Boca Raton.

Xiao, J., Xie, Y., Cao, H., 2015. Organic pollutants removal in wastewater by heterogeneous photocatalytic ozonation. Chemosphere 121, 1–17.

Yaghmaeian, K., Moussavi, G., Mashayekh-Salehi, A., Mohseni-Bandpei, A., Satari, M., 2017. Oxidation of acetaminophen in the ozonation process catalyzed with modified MgO nanoparticles: effect of operational variables and cytotoxicity assessment. Process Saf. Environ. Prot. 109, 520–528.

Zielinska-Jurek, A., Wysocka, I., Janczarek, M., Stampor, W., Hupka, J., 2015. Preparation and characterization of Pt–N/TiO_2 photocatalysts and their efficiency in degradation of recalcitrant chemicals. Sep. Purif. Technol. 156, 369–378.